ACS OMEGA

http://pubs.acs.org/journal/acsodf

Article

Ammonia Recovery from Wastewater as a Fuel: Effects of Supporting Electrolyte on Ammonium Permeation through a Cation-Exchange Membrane

Linji Xu, Dingyang Liu, Wenzong Liu, Jixiang Yang, Jiansheng Huang, Xinzhu Wang,* and Qiang He

Cite This: *ACS Omega* 2022, 7, 20634−20643

Read Online

ACCESS | Metrics & More | Article Recommendations | Supporting Information

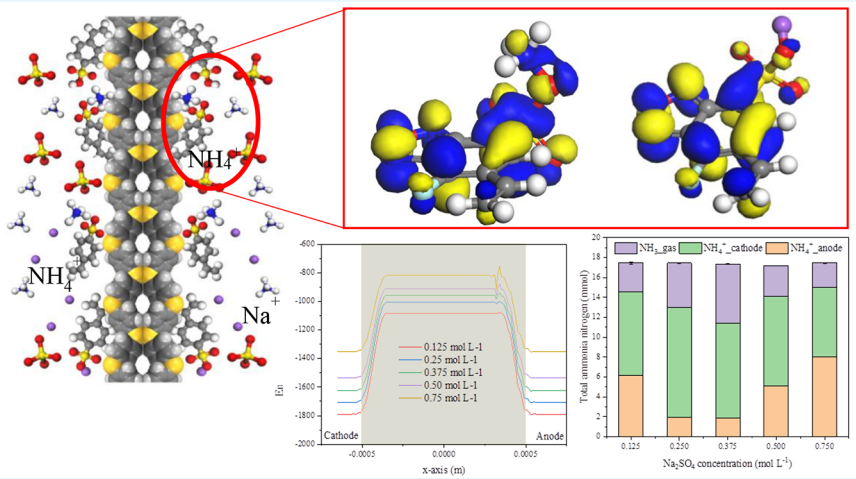

ABSTRACT: Electrodeionization (EDI) is used to recover ammonia from wastewater as a fuel, but how its performance for ammonia recovery is affected by the supporting electrolyte is not very clear. This study involved experimental tests and theoretical calculations on NH_3 recovery, NH_4^+ permeation, and NH_4^+ and Na^+ interacting with the functional groups in a cation exchange membrane (CEM) using Na_2SO_4 as the supporting electrolyte. The results demonstrated that a low concentration ($\leq$0.250 mol L^{-1} of Na_2SO_4) was conducive to NH_4^+ permeation, while the a concentration (0.750 mol L^{-1} of Na_2SO_4) hindered NH_4^+ permeation. A maximum recovery efficiency of ammonia of 80.00%, a current efficiency of 70.10%, and an energy balance ratio of 0.66 were obtained at 0.250 mol L^{-1} of Na_2SO_4. Numerical results indicated that an increase in Na_2SO_4 concentration caused severe concentration polarization that resisted NH_4^+ migration in the CEM. The DFT results demonstrated that competitive adsorption of Na^+ to the CEM hindered NH_4^+ migration. The weaker interacting force between NH_4^+ and the sulfonate functional group ($-SOH_3$) in comparison to that between Na^+ and $-SOH_3$ might be related to the geometric and orientation effects, which generated an additional energy barrier for NH_4^+ transport. Therefore, this study suggests that the supporting electrolyte concentration should be matched with that of the desalted ions.

1. INTRODUCTION

Ammonia (NH_3), occurring in wastewater and liquid waste from industry, municipalities, and agriculture has become the second-largest amount of pollutants after chemical oxygen demand (COD).[1] Overdischarged NH_3 entering water bodies results in environmental issues such as dissolved oxygen reduction, corrosion, disinfection inefficiencies, and toxicity to aquatic creatures.[2,3] Nevertheless, NH_3 is rich in H (17.60 wt % H) and has 5.2 kWh kg^{-1} energy intensity, 40% higher than that of methanol (12.60 wt % H, 4.32 kWh kg^{-1}), it is an attractive carbon-free fuel, and it has an essential role in energy storage and transportation.[4] NH_3 removal/recovery from wastewaters has attracted great effort by many scholars,[5,6] but it is either not easy to extract or the recovery efficiency is extremely low.[7,8]

Electrodeionization (EDI) is considered an effective approach for salt recovery, and it performs very well in ammonia recovery.[5,9−11] During ion separation, a supporting electrolyte is indispensable, since it provides sufficient

Received: February 3, 2022
Accepted: April 20, 2022
Published: June 7, 2022

electrolytic conductivity, reduces the Ohmic drop,[12−14] and releases the surface phenomena occurring between pollutant species and metal hydroxides.[15,16] It also enhances the ionic strength to form a compressed electric double layer (EDL) and generate a greater electric current in the circuit under a specific applied potential.[17,18] Meanwhile, the supporting electrolyte causes a problem in that it sometimes replaces the transport ion and becomes a determining factor, which greatly influences the concentration polarization of the ion exchange membrane.[19] According to the literature, the an inert or reactive supporting electrolyte concentration changed the limiting diffusion current density and led to an uneven electric current distribution.[20,21]

Additionally, the ions of the supporting electrolyte generally have more significant diffusion coefficients in comparison to the transport particles and form an extended DBL to hinder the target ion's transport and reduce the selective efficiency. Our study found that the Na_2SO_4 concentration caused fierce competition between Na^+ and NH_4^+ in the electric double layer (EDL). As a result, Na^+ formed a thin and compact layer to prevent NH_4^+ reduction, thus decreasing the hydrogen recovery.[9] We also found that NH_4^+ behaviors in the cathode were closely related to the NH_4^+ concentration.

However, the effects of the supporting electrolyte on NH_4^+ selectively migrating through cation exchange membrane (CEM) are still not fully understood. Therefore, in this paper, an extended study of the relationship between NH_4^+ permeation in a cation-exchange membrane and the supporting electrolyte is carried out through experimental tests and theoretical calculations. Na_2SO_4 is used as the supporting electrolyte because of its excellent performance.[22−25] We discuss NH_3 recovery, NH_4^+ permeation, and molecular interactions of NH_4^+, Na^+, and a functional group in a CEM based on ions permeating through polymeric membranes, an Arrhenius-type equation,[26,27] and density functional theory (DFT).[28,29] We hope that the results are helpful for EDI application on a full scale.

2. METHODS AND MATERIALS

2.1. Experimental Tests. *2.1.1. Electrodeionization Setup.* The EDI cell structure and the electrode material were the same as in our previous study.[9] A two-channel EDI reactor was made of an organic glass material. The effective volume of each channel was 20 mL. The anode and cathode were made of platinum plates with an area of 16 cm^2. The exchange membranes were IONSEP AM and IONSEP CM (IONTECH Co., Ltd., Shanghai, China). The diluted channel was fed into a 0.25 mol L^{-1} fixed $(NH_4)_2SO_4$ solution, and the concentrated channel was fed with 0.125, 0.250, 0.375, 0.500, 0.750 mol L^{-1} Na_2SO_4. An extra voltage of 2.0 V DC (PS-305DM, Hong Kong Longwei instrumentation Co., Ltd.) was applied to the EDI cell. All tests were conducted at 24.40−25.20 °C and 1.0 atm.

2.1.2. Chemical Analysis. The total gas generated from the cathode was collected in a gas bag then flowed through three serial cylinders with 1 mol L^{-1} H_2SO_4 solution. The ionized NH_3 and NH_4^+ were measured via the Berthelot method. The residual H_2 was determined by gas chromatography (Agilent 4890D; J&W Scientific, USA).[30] An HP-MoleSieve column (30 m × 0.53 mm × 50 m) was the detection column. Helium gas, the carrier gas, was injected at a rate of 6 mL min^{-1}. The injection port, column, and thermal conductivity detector temperatures were 200, 35, and 200 °C, respectively. Samples were injected by microsyringes with in 200 μL amounts (Shanghai Anting Scientific., China).

2.1.3. Electrochemical Impedance Spectroscopy and Current Measurements. Electrochemical impedance spectroscopy was used for measurements according to the method devised by Fu et al.[31] First, the membrane was immersed in 0.25 mol L^{-1} Na_2SO_4 for 24 h before each set of measurements.[25] Then, the impedances were recorded with frequencies ranging from 50 to 15000 kHz. Each point was repeated three times to minimize noise effects. Each point was repeated three times to minimize noise effects. The resistance was obtained based on fitted results as depicted in Supporting Information.

The current−voltage curve was measured on the basis of a method developed by Choi et al.[24] The cell was divided into two equal-volume (20 cm^3) compartments by a CEM. The anolyte $(NH_4)_2SO_4$ was fixed at 0.250 mol L^{-1}, and the concentration of the catholyte Na_2SO_4 was increased from 0.125 to 0.750 M. Anodic and cathodic channels were fed at a flow rate of 1.00 mL min^{-1}. A DC power source was added between the two Ag/AgCl electrodes. Then, a stepwise current supply was applied at a scanning rate of 30 mA min^{-1} through an electrochemical workstation (CorrWare, Scribner Associates Inc., USA). Finally, the electrodes were connected to a Keithley 2700 multimeter (Tektronix, Inc., USA). The potential drops of the two sides of the membrane were recorded and stored every 30 s.

2.2. Numerical Simulations and Calculations. The model was developed on the basis of one-dimensional transport phenomena. The initial concentrations of ions, flow rates, applied voltages, and membrane characteristics were input according to the characteristics of mustard tuber wastewater, the operating conditions, and the geometric structure. The principle of ion transport is displayed in Figure 1a. The assumed geometry of an electrolysis cell pair consisted of three parts (a diluted compartment, a concentrated compartment, and a cation-exchange membrane).[32−35] Since we only focused on the CEM, the numerical results near the membrane were plotted. The geometry of the cell was drawn using COMSOL Multiphysics version 5.4,[33] as shown in Figure 1b. Details of the calculations are described in the Supporting Information.

To simplify the numerical simulation, the process of the whole system maintained electroneutrality. Diffusivities and mobilities of the cation and anion are functions of the ion concentrations. The resistance of the ion exchange membrane was a function of both the salt concentration and time. The current densities of the ions are assumed to be equal to the current densities of the solutions at the interface of the membranes. No chemical reactions or water splitting were assumed even though the applied voltage reached 2.0 V.

2.2.1. Mass Transfer Phenomenon. Concentration diffusion and electrical migration are two forces that generate a concentration difference.[32] In this model, the Nernst−Planck−Poisson equation (NPP) is used in a two-dimensional mode to describe the ion flux and charge transport, as expressed by eq 1[33−35]

$$N_i = -D_i\nabla c_i - z_i u_i F c_i \nabla\phi + c_i v \quad (1)$$

where D_i is the diffusion coefficient, c_i is the concentration of the ions, $-D_i\nabla c_i$ is the diffusion flux, z_i is the charge, u_i is the species mobility, F is Faraday's constant, and φ is the

https://doi.org/10.1021/acsomega.2c00700
ACS Omega 2022, 7, 20634−20643

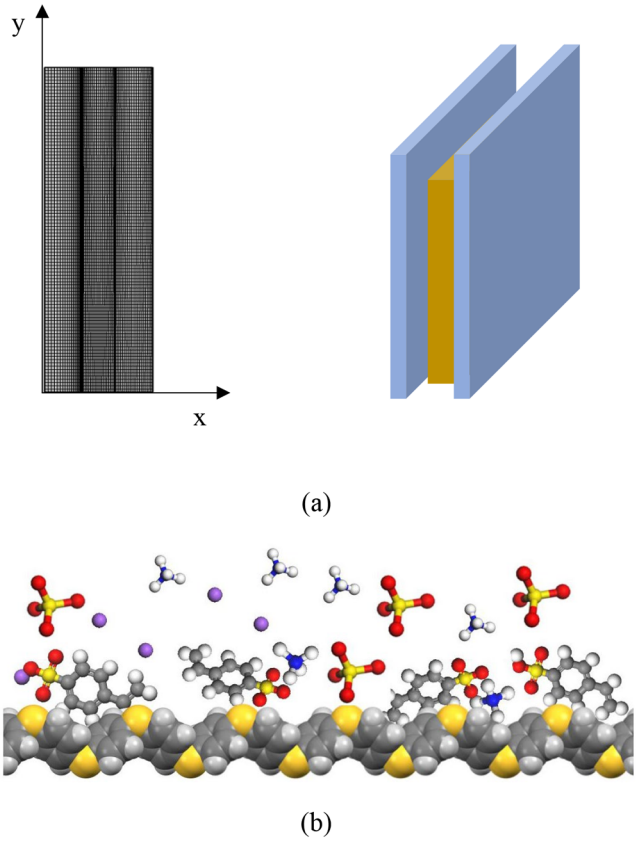

Figure 1. Ion transport through the membrane: (a) geometric structure and mesh used in numerical simulation; (b) polymer-sulfonate and solution.

electrolyte potential. In the convection term, v denotes the fluid velocity vector. i is NH_4^+, Na^+, or SO_4^{2-}.

2.2.2. Current Density. All of the molar fluxes should be used to calculate the electrolyte current density, but we ignored the convection term, and so the electrolyte current density is expressed by eq 2

$$i = F\sum_{i=1}^{n} z_i(-D_i\nabla c_i - z_i u_i F c_i \nabla\phi) \tag{2}$$

where the summation is made over all n ions. If ρ is the space charge density, then the current is given by eq 3:

$$\nabla\cdot i = \rho \tag{3}$$

The mesh building and solution study are available in the Supporting Information.

Current utilization (CU) and energy consumption (E) are two important parameters for EDI. CU is expressed through a control volume analysis for general electrolytes (eq 4)[36]

$$\mathrm{CU} = \frac{2\sum z\_c\_D\_}{\sum z\_c\_D\_ + \sum z_+c_+D_+} \tag{4}$$

where D is the diffusion coefficient, c is the concentration of the ions, and z is the charge carried by a cation/anion, respectively.

Substituting the electroneutrality equation (eq 5), current utilization is presented in eq 6.

$$z_+c_+ = z\_c\_ \tag{5}$$

$$\mathrm{CU} = \left.\frac{2D\_}{D\_ + D_+}\right|_{\text{EDI-CEMs}} = \left.\frac{2D_+}{D\_ + D_+}\right|_{\text{EDE-AEMs}} \tag{6}$$

Energy consumption (E_s) is used to compare the energies of different desalination devices. In electrochemical desalination systems, energy consumption is expressed by eq 7:

$$E_s = \frac{IV}{Q_{\text{desalted}}}\ \mathrm{Wh/L} \tag{7}$$

where I is the current, V is the voltage, and Q_{desalted} is the flow rate of desalted water.

Since energy consumption is a widely used metric determining the economic viability of a desalination technique, we consider energy consumption to remove a single pair of ions to more exactly describe the energy sonsumption. The energy per ion removal (E_{sp}) is given by eqs 8 and 9:

$$E_{sp} = \frac{IV/Q_{\text{desalted}}}{zk_BT(C_0 - C_{\text{desalted}})} = \frac{V^*}{\mathrm{CU}} \tag{8}$$

$$V^* = \frac{FV}{k_BT} \tag{9}$$

In unipolar EDI, EPIR/V^* is shifted to the opposite direction of the CU shift. z, F, k_B, and T indicate the ion valence, Faraday's constant (=9.65 × 10^4 C mol^{-1}), thermal energy (=2.479 kJ mol^{-1}; k_B, the Boltzmann constant) and temperature, respectively. V is the voltage, V^* is the nondimensionalized voltage, I is the current, N is the number of membrane pairs, C_0 is the initial ion concentration, C_{desalted} is the ion concentration of the desalted flow, and Q_{desalted} is the total desalted flow rate.

2.2.3. Energy Barrier. The energy barrier was calculated through an Arrhenius-type equation using single-salt solutions,[26] as given by eq 10

$$J = A\exp\left(-\frac{E_a}{RT}\right) \tag{10}$$

where J is the ion flux through the membrane, R is the universal gas constant, T is the absolute temperature, E_a the energy barrier, and A is the pre-exponential factor.

Then the natural logarithm of the ion flux, ln J, was plotted as a function of $1/T$, and the energy barrier (E_a) and pre-exponential factor (A) were determined from the linearized form of the Arrhenius-type equation (eq 11):

$$\ln J = \ln A - \frac{E_a}{R}\left(\frac{1}{T}\right) \tag{11}$$

2.3. Computational Details. The polymer sulfonate-ion unit was constructed in Materials Studio version 8.0 software, as shown in Figure 1b. The optimized geometry, electronic structure, and energy changes were calculated using the Dmol3 module.[37] GGA+PBE was used as the exchange correlation functional. A double-numerical basis set containing a polarization function (DNP) was employed for the calculations. The core treatment was set as semicore pseudopots to manage the interaction between the nucleus and valence electron. During the structure optimization, the k-point set of the Brillouin zone was 2 × 2 × 1 and the force convergence error was 0.02 hartree nm^{-1}. After the optimized geometric structure was obtained, the physical properties, including the density of states, frequency, and Fukui function, were calculated on the

https://doi.org/10.1021/acsomega.2c00700
ACS Omega 2022, 7, 20634−20643

basis of the optimized geometric structure. The *k*-point set was 24 × 24 × 1. Charges were analyzed using the Hirshfeld method.[29,38]

3. RESULTS

3.1. Ammonia Recovery from Solution. Driven by the applied electricity and concentration difference, NH_4^+ is transported from the anodic channel to the cathodic channel. As shown in Figure 2, when the concentration of Na_2SO_4

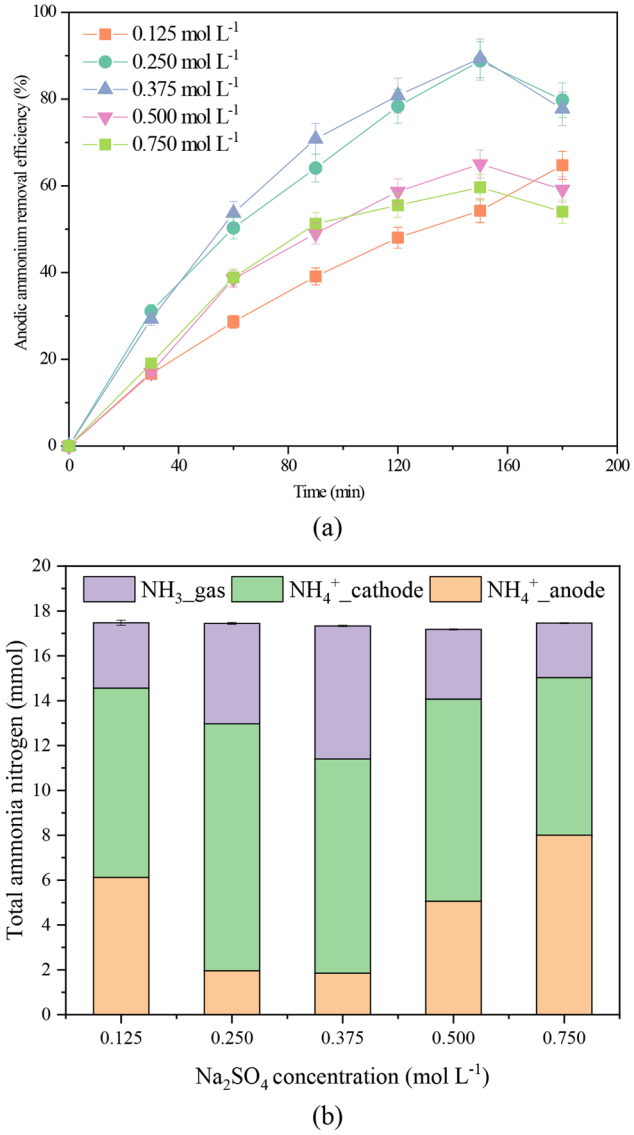

Figure 2. Ammonium conversion: (a) ammonium removal; (b) total ammonia nitrogen.

increases from 0.125 to 0.750 mol L^{-1}, the removal efficiencies of NH_4^+ climb to 54.25%, 88.80%, 89.41%, 65.01%, and 59.64% at 160 min but slightly decrease to 64.76%, 79.77%, 77.75%, 59.17%, and 54.03% at 180 min, respectively. The maximum removal efficiency of NH_4^+ is 79.77% at 0.250 mol L^{-1} of Na_2SO_4. This trend is thought to be caused by the different deionization rates, which increase to 5.83, 10.88, 10.25, 6.66, 5.94 mol L^{-1} h^{-1} within 30 min but gradually decrease to 1.171, 2.66, 2.01, 0.44, and 1.22 mol L^{-1} h^{-1} at 180 min, respectively (Figure 2a).

Since NH_4^+ migrating to the cathode was accompanied by water splitting, the generated OH^- combined NH_4^+ to produce $NH_3{\cdot}H_2O$ and further generated NH_3 under 2.00 V extra voltage. Therefore, the nitrogen element in the whole system existed in the forms of anodic NH_4^+, cathodic NH_4^+, NH_3 gas, and undetectable nitrogen, as discussed in our previous studies.[9,39] As shown in Figure 2b, the anodic amounts of NH_4^+ are 6.12, 1.96, 1.85, 5.06, and 8.00 mmol, respectively, and the cathodic amounts of NH_4^+ are 8.44, 11.01, 9.55, 9.01, and 7.03 nmol, respectively. With the anodic NH_4^+ migrating to the cathode, the converted NH_3 reaches 2.91, 5.93, 4.47, 1.41, and 2.43 mmol, respectively. The maximum NH_3 mass (5.93 mmol) is obtained at 0.25 mol L^{-1} Na_2SO_4. According to the nitrogen mass balance, it can be seen that a concentrated supporting electrolyte harms harms ammonia recovery.

3.2. Ammonium Permeation through a Cation Exchange Membrane. The above phenomena were thought to be caused by ion transport in the CEM and were further analyzed through numerical simulations. Since the conversion flux was ignored to simplify the calculations, the total flux consisting of the diffusion flux and migration flux in the direction along with the main component was analyzed. As plotted in Figure 3a, when the Na_2SO_4 concentration (0.125 mol L^{-1}) is lower than that of $(NH_4)_2SO_4$ (0.250 mol L^{-1}), the diffusion flux of NH_4^+ is positive, which means that the concentration potential transport predominantly drives NH_4^+. Conversely, when the Na_2SO_4 concentration equals the $(NH_4)_2SO_4$ concentration, the diffusion flux is close to zero, indicating that the electric force replaces the concentration potential as the dominant driving force. When the Na_2SO_4 concentration (>0.250 mol L^{-1}) is higher than the $(NH_4)_2SO_4$ concentration, the diffusion flux becomes negative, signifying that the concentration potential generated by Na^+ hinders NH_4^+ transport.

On consideration of electric migration, when the Na_2SO_4 concentration is lower than that of $(NH_4)_2SO_4$, the migration flux of NH_4^+ (absolute value) decreases to zero, as shown in Figure 3b). In contrast, with an increase in the Na_2SO_4 concentration, the migration flux of NH_4^+ dramatically increases from 0.004 m^2 s at 0.250 mol L^{-1} to 0.023 m^2 s at 0.750 mol L^{-1}, while its absolute value in EDL remains stable at 0.004 m^2 s as the Na_2SO_4 concentration (0.25 mol L^{-1}) equals that of $(NH_4)_2SO_4$ (0.25 mol L^{-1}). When the Na_2SO_4 concentration (0.375−0.750 mol L^{-1}) is higher than that of $(NH_4)_2SO_4$ (0.250 mol L^{-1}), the migration flux of NH_4^+ in absolute value in EDL decreases. The sum of diffusion and migration referring to total flux is illustrated in Figure 3c. The variations of NH_4^+ fluxes in EDL and DBL demonstrate that the diffusion flux of NH_4^+ has a positive increase with Na_2SO_4 concentration when the concentration of NH_4^+ is higher than that of the supporting electrolyte. The differences in fluxes finally result in changes in concentration and potential along with Na_2SO_4 concentration (Figures S1 and S2). It should be noted that the trend of NH_4^+ fluxes matches that of the measured potential.

On the basis of the total flux of NH_4^+, energy barriers of interaction between NH_4^+ and CEM were calculated and are plotted in Figure 3d. The energy barriers between the bulk solution and CEM for five concentration gradients are 708, 699, 664, 618, and 525 kcal mol^{-1}. A higher energy of the CEM indicates that the membrane shows earlier elution to the cation at equilibrium. The process of NH_4^+ exchange is faster than the cation in the membrane with lower energy.

https://doi.org/10.1021/acsomega.2c00700
ACS Omega 2022, 7, 20634−20643

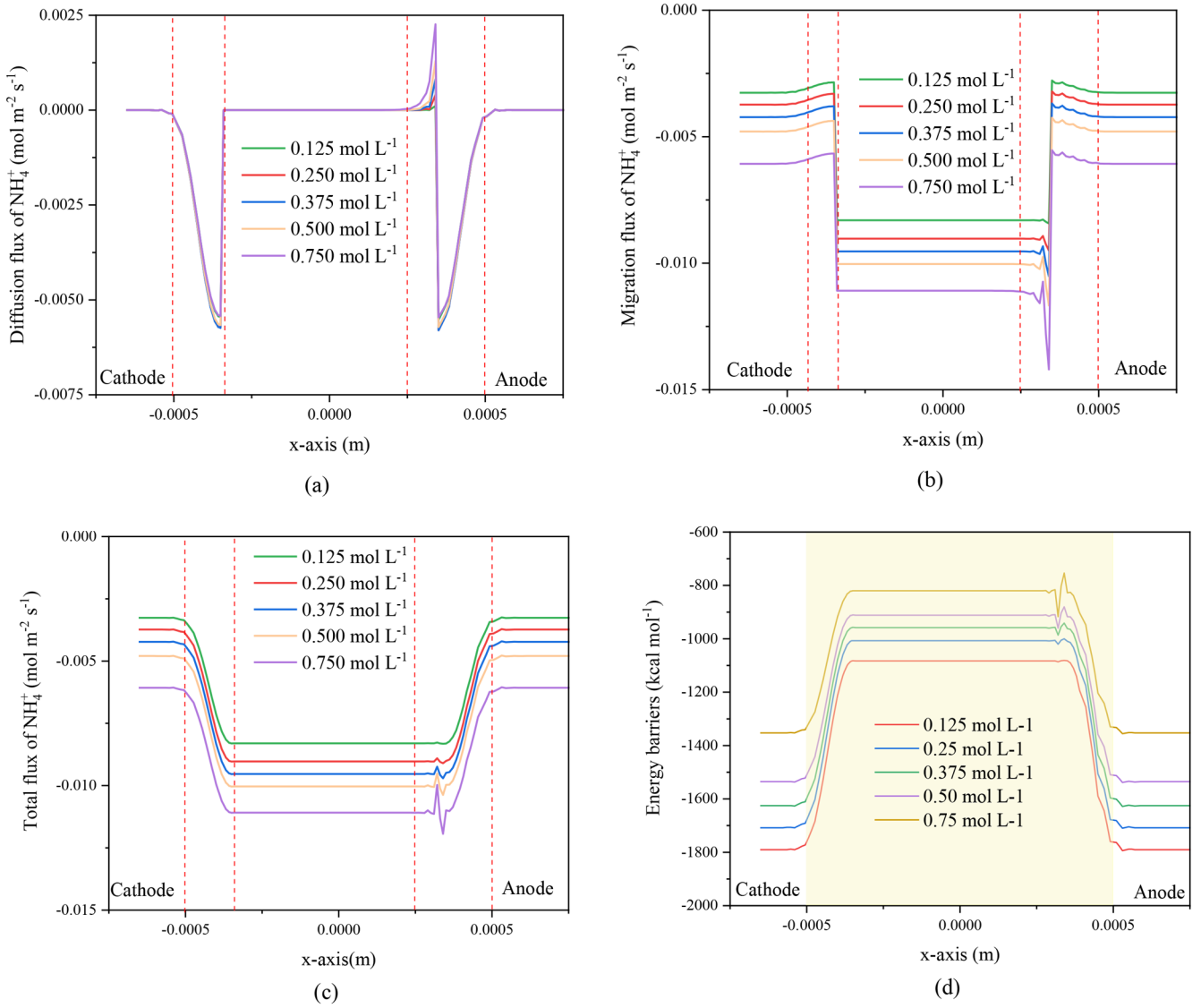

Figure 3. NH_4^+ fluxes and energy barriers: (a) diffusive flux; (b) migrative flux; (c) total flux; (d) energy barriers.

Additionally, it can be seen that the zigzags of migration flux become increasingly evident with the supporting electrolyte concentration. We imagine that this phenomenon might be related to the mesh and the supporting electrolyte concentration. During calculations, it was found that a finer mesh gave smaller zigzags. However, the finer the mesh was set, the harder it was for the model to converge. Therefore, the mesh was adjusted to make sure that the model was converged. However, zigzags could not be completely eliminated. This phenomenon indicates that the model needs to be improved when it is used to study concentrated ion migration.

3.3. Ammonium Interaction with Functional Group. The interaction between permeable NH_4^+ and the CEM was studied via theoretical calculations. The structures of polymer sulfonate-acid, polymer sulfonate-ammonium, and polymer sulfonate-sodium units were built and optimized in Materials Studio software (Figure 4). The DFT-calculated length information on more bonds at the minimum energy state is given in Table 1. In detail, the original O4−N and O4−Na bond lengths in the functional group ($-SO_3H$) were 1.480 and 2.401 Å, respectively. After geometric optimization, the bond lengths decreased to 1.473 and 1.168 Å, respectively. These obtained lengths are in good agreement with the results reported in the literature.[29]

Bond lengths reflect the polymer sulfonate-ion bound structure's mechanical and chemical stability.[40,41] A shorter bond signifies that more energy to break it is required. According to Table 2, the bond length of the $-SO_3H$ group interacting with Na^+ is much shorter than that with NH_4^+, indicating that Na^+ is more accessible than NH_4^+ in the membrane. The simulated chemical structures at the minimum energy state, along with their HOMO and LUMO frontier orbitals, are shown in Figure 5. The energies of the highest occupied molecular orbital for NH_4^+ and Na^+ combined with sulfonate are −5.946 and −5.190 eV, and the energies of the lowest unoccupied molecular orbital are −4.160 and −4.370 eV, respectively. Polymer sulfonate-NH_4^+ and polymer sulfonate-Na^+ units exhibit band gaps of 1.786 and 0.820 eV, respectively. Generally, the larger the energy gap between the frontier orbitals, the more difficult it is to transfer electrons from the HOMO to the LUMO because the activity increases as the energy gap decreases. The energy gap demonstrates that

https://doi.org/10.1021/acsomega.2c00700
ACS Omega 2022, 7, 20634−20643

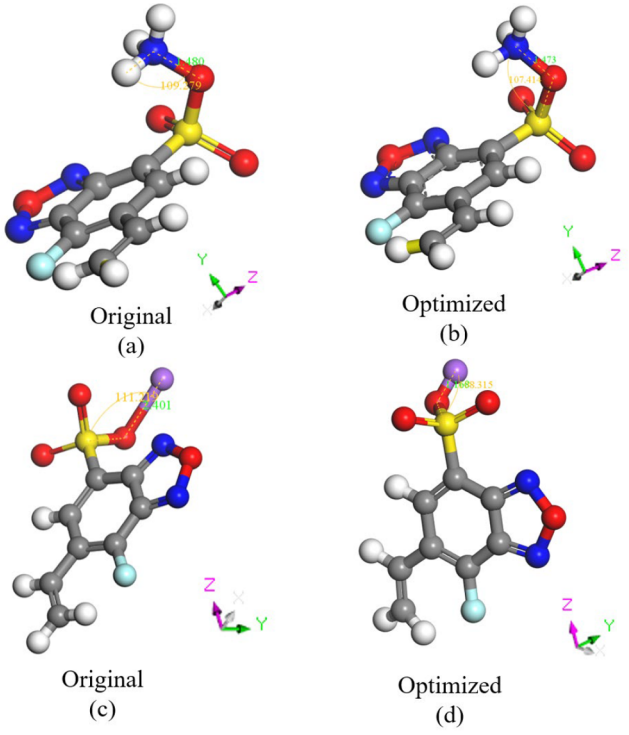

Figure 4. Polymer sulfonate-ion unit: (a) original polymer sulfonate-NH_4^+; (b) optimized polymer sulfonate-NH_4^+; (c) original polymer sulfonate-Na^+; (d) optimized polymer sulfonate-Na^+.

Table 1. Most Relevant Bond Lengths (Å)

bond	polymer sulfonate-acid	polymer sulfonate-ammonium	polymer sulfonate-sodium
C−N	1.140	1.082	1.110
C−N	1.140	1.079	1.111
H17−C	1.337	1.354	1.409
C15−H17	1.447	1.419	1.471
C13−C15	1.432	1.395	1.441
C14−C15	1.377	1.458	1.441
F2−C14	1.326	1.333	1.397
N8−C12	1.320	1.332	1.393
O3−N8	1.350	1.392	1.427
O3−N7	1.356	1.418	1.428
N7−C11	1.315	1.308	1.390
S1−C10	1.753	1.771	1.771
S1−O5	1.438	1.444	1.714
S1−O4	1.604	1.506	1.635
	1.110 (O4−H18)	1.473 (O4−N)	1.168 (O4−Na)
		1.010 (N−H)	

Na^+ combined with SO_3H groups has a higher chemical and mechanical stability in comparison to NH_4^+.

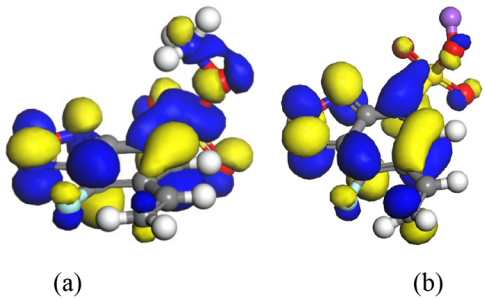

Figure 5. Chemical structures simulated in this work, along with the spatial distributions of their frontier HOMO and LUMO orbitals: (a) polymer sulfonate-NH_4^+; (b) polymer sulfonate-Na^+.

Moreover, Na^+ has a smaller radius but a larger diffusion coefficient than NH_4^+. Its interaction force with CEM is much stronger than that of NH_4^+, indicating that more favorably adsorbed ions with higher affinity to the polymer matrix have lower diffusion within the membrane: e.g., Na^+ was more favorably adsorbed than NH_4^+ but diffused more slowly through the membrane. Na^+ had stronger attractive bonds with the fixed groups in the polymer matrix that inhibited its diffusion within the membrane in comparison to NH_4^+. Moreover, NH_4^+ has a central nitrogen atom surrounded by four hydrogen atoms in a tetrahedral geometry. This structure consists of four equally spaced sp^3 hybrid orbitals forming a tetrahedral geometry with bond angles of 109.5°, which is an asymmetrical 3D structure. A rotation around any axis may result in a molecule indistinguishable from the original. The differences in electron densities around the molecule can render some areas on the surface sterically less approachable than others. Therefore, the geometric and orientation effects may impose an additional energy barrier for NH_4^+ transport.[26] These results further explain why the excess concentration of supporting electrolyte hinders the target ion transport in an ion exchange membrane.

4. DISCUSSION

4.1. Ammonia Recovery Related to Current Utilization and Energy Balance. On the basis of the recovered ammonia mass and consumed energy, the current utilization, current efficiency, and energy balance were analyzed and are summarized in Table 1. Apparently, the current utilization slightly increase with an increase in Na_2SO_4 concentration, signifying that the concentration of the supporting electrolyte has almost no effect on the Coulombic efficiency when the conductivity of the bulk solution is high enough.[42] However, the current efficiency had an upward trend to 70.10% at 0.25 mol L^{-1} Na_2SO_4 and then a dramatic downward trend to 37.65% at 0.75 mol L^{-1} Na_2SO_4. The decrease in current efficiency indicates that there is a lower actual mass of a substance liberated from an electrolyte by the current in

Table 2. Energy Balance Evaluation

Na_2SO_4 concn, mol L^{-1}	current utilization, %	current efficiency, %	energy potential (NH_3), J	energy consumption (total), J	energy balance
0.125	78.53	58.23	931.21	1629.39	0.57
0.250	81.78	70.10	1898.44	2886.92	0.66
0.375	83.51	62.17	1430.36	2302.64	0.62
0.500	84.58	46.84	450.42	1629.30	0.28
0.750	85.85	37.65	776.60	1921.34	0.40

https://doi.org/10.1021/acsomega.2c00700
ACS Omega 2022, 7, 20634−20643

comparison to the theoretical mass, which is generally thought to be affected by increasingly severe concentration polarization.[43] In this study, the recovered NH_3 increases with Na_2SO_4 concentration when the real current is under the limiting current density. Moreover, Na^+ migration is an ignorable factor due to supporting ions sharing the current, explaining the reason the current efficiency decreases with Na_2SO_4 concentration. Due to the differences in current efficiencies and consumed energies, it can be seen that a maximum energy balance of 0.66 is obtained at 0.25 M, which signifies that the recovered NH_3 cannot achieve an offset of energy consumption and still needs 34% of energy input.

Figure 6a,b display the current density and potential crossing the membrane. Specifically, the current density increases from 2.98 mA cm^{-2} at 0.125 mol L^{-1} to 5.63 mA cm^{-2} at 0.750 mol L^{-1}. In contrast, the potential decreases from 0.0086 to −0.016 V at the corresponding Na_2SO_4 concentration. Since the changes in the current and potential further resulted in resistance differences, the electric resistance of the whole system was analyzed with the aid of EIS. For EDI, the total resistance $\mathcal{R}_{tot}$ equals the sum of the resistance of the solution ($\mathcal{R}_{sol}$), the resistance of the membrane ($\mathcal{R}_{mem}$), the resistance of the diffusion layer ($\mathcal{R}_{diff}$), the resistance of the Donnan interfacial layer ($\mathcal{R}_{don}$), and the resistance of the electrode ($\mathcal{R}_{el}$)[25] (eq 12).

$$\mathcal{R}_{tot} = \mathcal{R}_{sol} + \mathcal{R}_{mem} + \mathcal{R}_{diff} + \mathcal{R}_{don} + \mathcal{R}_{el} \quad (12)$$

The perturbation frequency ranges are usually divided into three regions (high-, medium-, and low-frequency ranges). Each region reflects its corresponding resistance. In the high-frequency ranges, the total impedance of the membrane system is expressed as eq 13:[44,45]

$$Z_{tot}(\omega) = \mathcal{R}_{mem} + \mathcal{R}_{sol} \quad (13)$$

In low-frequency ranges, the total resistance is expressed as eq 14:

$$Z_{tot}(\varpi) = \left(\mathcal{R}_{mem} + \mathcal{R}_{sol} + \frac{\mathcal{R}_{don}}{1 + \varpi^2 c_{don}^2 \mathcal{R}_{don}^2} + \frac{\mathcal{R}_{diff}}{1 + \varpi^2 c_{diff}^2 \mathcal{R}_{diff}^2}\right) - \left(\frac{c_{don}\mathcal{R}_{don}^2}{1 + \varpi^2 c_{don}^2 \mathcal{R}_{don}^2} + \frac{c_{diff}\mathcal{R}_{diff}^2}{1 + \varpi^2 c_{diff}^2 \mathcal{R}_{diff}^2}\right)\varpi j \quad (14)$$

$\mathcal{R}_{el}$ and $\mathcal{R}_{don}$ are negligible; thus, eq 14 is simplified to eq 15

$$Z_{tot}(\varpi) = \left(\mathcal{R}_{mem} + \mathcal{R}_{sol} + \frac{\mathcal{R}_{diff}}{1 + \varpi^2 c_{diff}^2 \mathcal{R}_{diff}^2}\right) - \left(\frac{c_{diff}\mathcal{R}_{diff}^2}{1 + \varpi^2 c_{diff}^2 \mathcal{R}_{diff}^2}\right)\varpi j \quad (15)$$

where $j = \sqrt{-1}$.

The fitting resistances for the different parts are illustrated in Figure 6c. The electric resistance of a solution apparently decreases from 25.9 Ω at 0.125 mol L^{-1} to 13.93 Ω at 0.75 mol L^{-1}, while that of the membrane slightly increases from 8.22 to 8.54 Ω. The resistance of the diffusion layer experiences a dramatic drop to 2.5 Ω and then an increase to 16.0 Ω. The total resistances are 41.70, 32.00, 32.40, 37.29, and 38.50 Ω, respectively. The variation of electric resistance indicates that

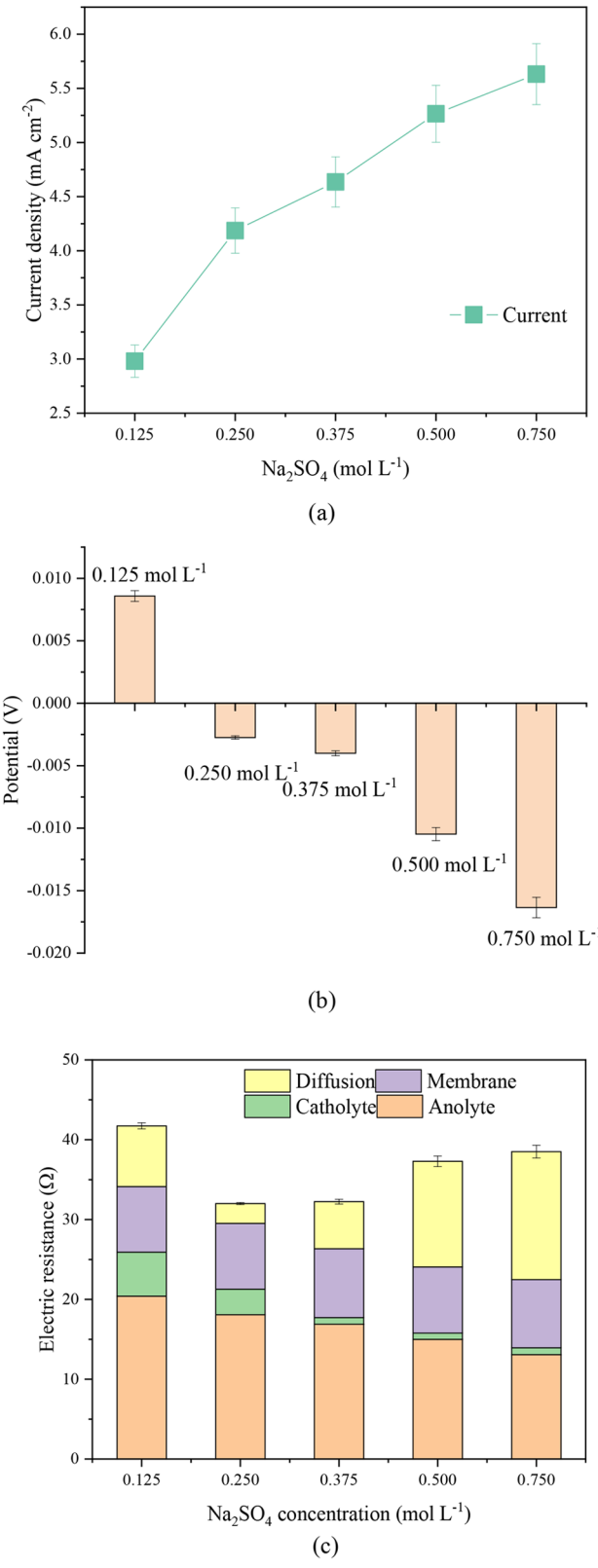

Figure 6. Electric properties: (a) real current density; (b) membrane potential; (c) electric resistance.

increasing the supporting electrolyte concentration indeed reduces the Ohmic resistance for the dilute condition, which is related to the ionic conductivity and viscosity of the bulk solution. In contrast, the concentrated supporting electrolyte

https://doi.org/10.1021/acsomega.2c00700
ACS Omega 2022, 7, 20634−20643

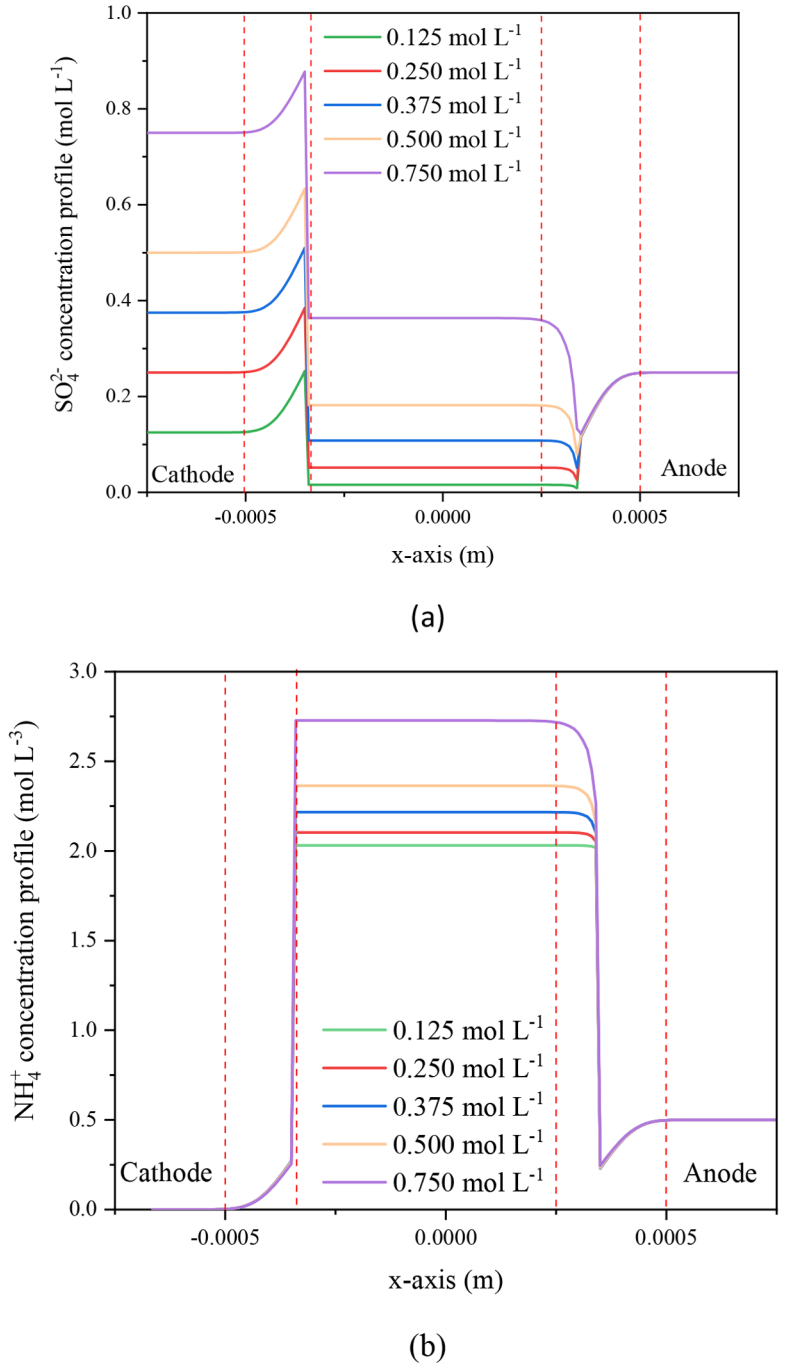

Figure 7. Concentration distribution near CEM: (a) SO_4^{2-} concentration profile; (b) NH_4^+ concentration profile.

makes concentration polarization much easier to occur. This finding is critical for practical engineering, since the concentrated channel undergoes serious concentration polarization, leading to much more energy consumption and poorer desalination capability. Therefore, it is significant to keep a rational concentration of the supporting electrolyte to improve desalination efficiency.

4.2. Ammonia Recovery Hindered by Concentration Polarization of SO_4^{2-}. According to the achieved results, NH_4^+ transport through the CEM was closely related to the Na_2SO_4 concentration. Ammonium ion exchange mainly occurred at the interfaces, and the exchange process was short and fast. As a result, the aggregate amount of ammonium at the interface was much larger than the amount in the membrane. Therefore, the concentration of ammonium in the membrane seems to be unchanged. On consideration of SO_4^{2-}, Na_2SO_4 dissociated in the solvent and formed the electrochemically stable complex Na^+ and SO_4^{2-} to provide current transport through the solution and CEM. SO_4^{2-} has a different interaction with the CEM in comparison to Na^+. As plotted in Figure 7, SO_4^{2-} forms a thick diffusion layer at the interface of the CEM and the cathode bulk solution. The thickness of the diffusion layer increases with Na_2SO_4 concentration, caused by concentration and electric potential gaps. An increase in the difference of the concentration between the anolyte and the catholyte serves as a force to drive SO_4^{2-} diffusion. Although

https://doi.org/10.1021/acsomega.2c00700
ACS Omega 2022, 7, 20634−20643

SO_4^{2-} migrates in the direction of the anode in the electric field, it cannot go through the CEM. As a result, the accumulation of SO_4^{2-} forms a thick diffusion layer. SO_4^{2-} clearly shows a Donnan exclusion effect due to permanent negative charges at the CEM surface. SO_4^{2-} has slower migration and effective diffusion coefficient than NH_4^+.[46,47] Even though the electric force cannot drive Na^+ migration to the CEM, its concentration potential is large enough to impose a strong force so that Na^+ carrying a positive charge is adsorbed by the anion in CEM.

5. CONCLUSION

This study investigated Na_2SO_4 as the supporting electrolyte affecting ammonia recovery from nitrogenous wastewaters. Experimental tests and theoretical simulations demonstrated that Na_2SO_4 conditionally improved ammonia recovery. Increasing the Na_2SO_4 concentration in the dilute range ($\leq$0.250 mol L^{-1}) accelerated NH_4^+ transport. As the Na_2SO_4 concentration was further increased, the current efficiency and energy balance ratio decreased. The maximum recovery efficiency of 80.00%, current efficiency of 70.10%, and energy balance ratio of 0.66 were obtained at 0.250 mol L^{-1} of Na_2SO_4. Thus, the feasible concentration of Na_2SO_4 in this study was 0.250 mol L^{-1}. The exchange process of ions in the membrane was determined by the diffusion layer formed by SO_4^{2-} and the interaction energy. The thick diffusion layer resisted NH_4^+ transport through the CEM. Na^+ competitively interacted with $-SO_3H$ groups to produce a high chemical and mechanical stability, hindering NH_4^+ migration. The geometrt and orientation of NH_4^+ might generate an additional energy barrier for NH_4^+ transport. Therefore, this study suggests that the supporting electrolyte plays an essential role in EDI and controlling a rational concentration is conducive for NH_3 recovery via EDI.

■ ASSOCIATED CONTENT

Supporting Information

The Supporting Information is available free of charge at https://pubs.acs.org/doi/10.1021/acsomega.2c00700.

Numerical simulation process and additional experimental results (PDF)

■ AUTHOR INFORMATION

Corresponding Author

Xinzhu Wang − *Chongqing Key Laboratory of Heterogeneous Material Mechanics, College of Aerospace Engineering, Chongqing University, Chongqing 400040, People's Republic of China*; Phone: +86-15334520880; Email: wxz@cqu.edu.cn

Authors

Linji Xu − *Faculty of Environment and Ecology, Chongqing University, Chongqing 400044, People's Republic of China*; orcid.org/0000-0002-7632-2933

Dingyang Liu − *Chongqing Key Laboratory of Heterogeneous Material Mechanics, College of Aerospace Engineering, Chongqing University, Chongqing 400040, People's Republic of China*

Wenzong Liu − *School of Civil and Environmental Engineering, Harbin Institute of Technology Shenzhen, Shenzhen 518055, People's Republic of China*

Jixiang Yang − *Key Laboratory of Reservoir Aquatic Environment, Chongqing Institute of Green and Intelligent Technology, Chinese Academy of Sciences, Chongqing 401174, People's Republic of China*

Jiansheng Huang − *School of Chemistry and Chemical Engineering, Chongqing University of Science and Technology, Chongqing 401331, People's Republic of China*

Qiang He − *Faculty of Environment and Ecology, Chongqing University, Chongqing 400044, People's Republic of China*

Complete contact information is available at: https://pubs.acs.org/10.1021/acsomega.2c00700

Notes

The authors declare no competing financial interest.

■ ACKNOWLEDGMENTS

The authors wish to acknowledge the National Natural Science Foundation of China (U20A20326), the Science Foundation of the National Key Laboratory of Science and Technology on Advanced Composites in Special Environments (No. 6142905202711), the State Key Laboratory for the Modification of Chemical Fibers and Polymer Materials (No. KF2119), and the Venture & Innovation Support Program for Chongqing Overseas Returnees (No. cx2020001) for providing financial support.

■ REFERENCES

(1) Soloveichik, G. In *Future of ammonia production: improvement of Haber-Bosch process or electrochemical synthesis AIChE annu. Meet. Top. Conf. Minneapolis: NH3 Energy*, 2017.

(2) Lauterböck, B.; Ortner, M.; Haider, R.; Fuchs, W. Counteracting ammonia inhibition in anaerobic digestion by removal with a hollow fiber membrane contactor. *Water Res.* **2012**, *46* (15), 4861−4869.

(3) Krakat, N.; Demirel, B.; Anjum, R.; Dietz, D. Methods of ammonia removal in anaerobic digestion: a review. *Water Sci. Technol.* **2017**, *76* (8), 1925−1938.

(4) Yang, K.; Liu, J.; Yang, B. Electrocatalytic oxidation of ammonia on Pt: Mechanistic insights into the formation of N2 in alkaline media. *J. Catal.* **2022**, *405*, 626−633.

(5) Chen, T.-L.; Chen, L.-H.; Lin, Y. J.; Yu, C.-P.; Ma, H.-w.; Chiang, P.-C. Advanced ammonia nitrogen removal and recovery technology using electrokinetic and stripping process towards a sustainable nitrogen cycle: a review. *J. Clean. Prod.* **2021**, *309*, 127369.

(6) Ghavam, S.; Vahdati, M.; Wilson, I.; Styring, P. Sustainable ammonia production processes. *Front. Energy Res.* **2021**, *9*, 34.

(7) Khasani; Prasidha, W.; Widyatama, A.; Aziz, M. Energy-saving and environmentally-benign integrated ammonia production system. *Energy* **2021**, *235*, 121400.

(8) Cruz, H.; Law, Y. Y.; Guest, J. S.; Rabaey, K.; Batstone, D.; Laycock, B.; Verstraete, W.; Pikaar, I. Mainstream ammonium recovery to advance sustainable urban wastewater management. *Environ. Sci. Technol.* **2019**, *53* (19), 11066−11079.

(9) Xu, L.; Pang, Y.; Huang, D.; Zhuang, H.; Luo, T.; Lee, P.-H.; Liu, W.; Zhang, S.; Feng, L. Increasing ammonia recovery from high-level ammonium wastewater via adding sodium sulfate to prevent nitrogen generation in the cathode. *Environ. Res.* **2020**, *186*, 109521.

(10) Zheng, H.; Gong, X.; Yang, Y.; Yang, J.; Yang, X.; Wu, Z. Concentration of nitrogen as new energy source from wastewater by electrodeionization. *Energy Procedia* **2017**, *142*, 1421−1426.

(11) Tanaka, Y. *Ion exchange membranes: fundamentals and applications*; Elsevier: 2015.

(12) Zheng, J.; Lochala, J. A.; Kwok, A.; Deng, Z. D.; Xiao, J. Research progress towards understanding the unique interfaces between concentrated electrolytes and electrodes for energy storage applications. *Adv. Sci.* **2017**, *4* (8), 1700032.

(13) Xu, K. Nonaqueous liquid electrolytes for lithium-based rechargeable batteries. *Chem. Rev.* **2004**, *104* (10), 4303−4418.
(14) Sharma, P.; Bhatti, T. A review on electrochemical double-layer capacitors. *Energy Convers. Manag.* **2010**, *51* (12), 2901−2912.
(15) Izquierdo, C. J.; Canizares, P.; Rodrigo, M.; Leclerc, J.; Valentin, G.; Lapicque, F. Effect of the nature of the supporting electrolyte on the treatment of soluble oils by electrocoagulation. *Desalination* **2010**, *255* (1), 15−20.
(16) Tsierkezos, N. G.; Ritter, U. Influence of concentration of supporting electrolyte on electrochemistry of redox systems on multi-walled carbon nanotubes. *Phys. Chem. Liq.* **2012**, *50* (5), 661−668.
(17) Gritzner, G. Influence of the supporting electrolyte on standard electrode reaction rate constants on mercury. *J. Solid State Electrochem.* **2004**, *8* (10), 757−762.
(18) Yıldız, Y. S.; Koparal, A. S.; Keskinler, B. Effect of initial pH and supporting electrolyte on the treatment of water containing high concentration of humic substances by electrocoagulation. *J. Chem. Eng.* **2008**, *138* (1-3), 63−72.
(19) Vermaas, D. A.; Wiegman, S.; Nagaki, T.; Smith, W. A. Ion transport mechanisms in bipolar membranes for (photo) electrochemical water splitting. *Sustain. Energy Fuels* **2018**, *2* (9), 2006−2015.
(20) Tanaka, Y. Concentration polarization in ion-exchange membrane electrodialysis: The events arising in an unforced flowing solution in a desalting cell. *J. Membr. Sci.* **2004**, *244* (1-2), 1−16.
(21) Tanaka, Y. Concentration polarization in ion-exchange membrane electrodialysis—the events arising in a flowing solution in a desalting cell. *J. Membr. Sci.* **2003**, *216* (1), 149−164.
(22) Fierro, S.; Honda, Y.; Einaga, Y. Influence of supporting electrolyte on the electrochemical oxidation of formic acid on boron-doped diamond electrodes. *Bull. Chem. Soc. Jpn.* **2013**, *86* (6), 749−754.
(23) Güler, E.; van Baak, W.; Saakes, M.; Nijmeijer, K. Monovalent-ion-selective membranes for reverse electrodialysis. *J. Membr. Sci.* **2014**, *455*, 254−270.
(24) Choi, J.-H.; Park, J.-S.; Moon, S.-H. Direct measurement of concentration distribution within the boundary layer of an ion-exchange membrane. *J. Colloid Interface Sci.* **2002**, *251* (2), 311−317.
(25) Wang, Y.; Wang, A.; Zhang, X.; Xu, T. The concentration, resistance, and potential distribution across a cation exchange membrane in 1:2 (Na 2 SO 4) type aqueous solution. *Desalination* **2012**, *284*, 106−115.
(26) Epsztein, R.; Shaulsky, E.; Qin, M.; Elimelech, M. Activation behavior for ion permeation in ion-exchange membranes: Role of ion dehydration in selective transport. *J. Membr. Sci.* **2019**, *580*, 316−326.
(27) Badessa, T.; Shaposhnik, V. The electrodialysis of electrolyte solutions of multi-charged cations. *J. Membr. Sci.* **2016**, *498*, 86−93.
(28) Zelovich, T.; Vogt-Maranto, L.; Hickner, M. A.; Paddison, S. J.; Bae, C.; Dekel, D. R.; Tuckerman, M. E. Hydroxide ion diffusion in anion-exchange membranes at low hydration: insights from ab initio molecular dynamics. *Chem. Mater.* **2019**, *31* (15), 5778−5787.
(29) López-Chávez, E.; Peña-Castañeda, Y. A.; de la Portilla-Maldonado, L. C.; Guzmán-Pantoja, J.; Martínez-Magadán, J. M.; Oviedo-Roa, R.; de Landa Castillo-Alvarado, F.; Cruz-Torres, A. Role of sulfonation in the stability, reactivity, and selectivity of poly (ether imide) used to develop ion exchange membranes: DFT study with application to fuel cells. *J. Mol. Model.* **2014**, *20* (7), 1−9.
(30) Ramió-Pujol, S.; Ganigué, R.; Bañeras, L.; Colprim, J. Incubation at 25 Celsius prevents acid crash and enhances alcohol production in Clostridium carboxidivorans P7. *Bioresour. Technol.* **2015**, *192*, 296−303.
(31) Fu, R.-Q.; Xu, T.-W.; Cheng, Y.-Y.; Yang, W.-H.; Pan, Z.-X. Fundamental studies on the intermediate layer of a bipolar membrane: Part III. Effect of starburst dendrimer PAMAM on water dissociation at the interface of a bipolar membrane. *J. Membr. Sci.* **2004**, *240* (1), 141−147.
(32) Sistat, P.; Pourcelly, G. Chronopotentiometric response of an ion-exchange membrane in the underlimiting current-range. Transport phenomena within the diffusion layers. *J. Membr. Sci.* **1997**, *123* (1), 121−131.
(33) Bawornruttanaboonya, K.; Devahastin, S.; Yoovidhya, T.; Chindapan, N. Mathematical modeling of transport phenomena and quality changes of fish sauce undergoing electrodialysis desalination. *J. Food Eng.* **2015**, *159*, 76−85.
(34) Burt, R.; Birkett, G.; Zhao, X. S. A review of molecular modelling of electric double layer capacitors. *Phys. Chem. Chem. Phys.* **2014**, *16*, 6519−6538.
(35) Moshtarikhah, S.; Oppers, N.; de Groot, M.; Keurentjes, J.; Schouten, J.; van der Schaaf, J. Nernst−Planck modeling of multicomponent ion transport in a Nafion membrane at high current density. *J. Appl. Electrochem.* **2017**, *47* (1), 51−62.
(36) Kwak, R.; Pham, V. S.; Kim, B.; Chen, L.; Han, J. Enhanced salt removal by unipolar ion conduction in ion concentration polarization desalination. *Sci. Rep.* **2016**, *6* (1), 1−11.
(37) Abdulfatai, U.; Uzairu, A.; Uba, S.; Shallangwa, G. A. Quantitative structure-properties relationship, molecular dynamic simulations and designs of some novel lubricant additives. *Egypt. J. Pet.* **2019**, *28* (2), 241−245.
(38) Biabangard, F.; Nazari, H.; Arefinia, R. Effect of pH on the electrochemical properties of polyaniline nanoparticle suspension in strongly acidic solution: an experimental and theoretical study. *J. Solid State Electrochem.* **2021**, *25* (3), 881−893.
(39) Xu, L.; Dong, F.; Zhuang, H.; He, W.; Ni, M.; Feng, S.-P.; Lee, P.-H. Energy upcycle in anaerobic treatment: Ammonium, methane, and carbon dioxide reformation through a hybrid electrodeionization−solid oxide fuel cell system. *Energy Conversion and Management* **2017**, *140*, 157−166.
(40) Ganie, A. A.; Marimuthu, R.; Islam, S. T.; Narang, S.; Dar, A. A. Molecular salts of the isoniazid derivatives. Expanding the scope of sulfonate-pyridinium synthon to design materials. *J. Solid State Chem.* **2022**, *307*, 122762.
(41) Thuc, V. D.; Tinh, V. D. C.; Kim, D. Simultaneous improvement of proton conductivity and chemical stability of Nafion membranes via embedment of surface-modified ceria nanoparticles in membrane surface. *J. Membr. Sci.* **2022**, *642*, 119990.
(42) Doornbusch, G.; Swart, H.; Tedesco, M.; Post, J.; Borneman, Z.; Nijmeijer, K. Current utilization in electrodialysis: Electrode segmentation as alternative for multistaging. *Desalination* **2020**, *480*, 114243.
(43) Long, R.; Wu, F.; Chen, X.; Liu, Z.; Liu, W. Temperature-depended ion concentration polarization in electrokinetic energy conversion. *Int. J. Heat Mass Transfer* **2021**, *168*, 120842.
(44) Freger, V.; Bason, S. Characterization of ion transport in thin films using electrochemical impedance spectroscopy: I. Principles and theory. *J. Membr. Sci.* **2007**, *302* (1−2), 1−9.
(45) Bason, S.; Oren, Y.; Freger, V. Characterization of ion transport in thin films using electrochemical impedance spectroscopy: II: Examination of the polyamide layer of RO membranes. *J. Membr. Sci.* **2007**, *302* (1−2), 10−19.
(46) Van Loon, L.; Glaus, M.; Ferry, C.; Latrille, C., Studying radionuclide migration on different scales: the complementary roles of laboratory and in situ experiments. In *Radionuclide Behaviour in the Natural Environment*; Elsevier: 2012; pp 446−483.
(47) Petsev, D. N. *Emulsions: structure, stability and interactions*. Elsevier: 2004.

https://doi.org/10.1021/acsomega.2c00700
ACS Omega 2022, 7, 20634−20643